frontiers in Chemistry

ORIGINAL RESEARCH
published: 06 November 2018
doi: 10.3389/fchem.2018.00540

Electrospun ZnO–SnO_2 Composite Nanofibers and Enhanced Sensing Properties to SF_6 Decomposition Byproduct H_2S

Zhaorui Lu[1], *Qu Zhou*[1,2*], *Caisheng Wang*[2*], *Zhijie Wei*[1], *Lingna Xu*[1] *and Yingang Gui*[1]

[1] College of Engineering and Technology, Southwest University, Chongqing, China, [2] Electrical and Computer Engineering Department, Wayne State University, Detroit, MI, United States

Hydrogen sulfide (H_2S) is an important decomposition component of sulfur hexafluoride (SF_6), which has been extensively used in gas-insulated switchgear (GIS) power equipment as insulating and arc-quenching medium. In this work, electrospun ZnO-SnO_2 composite nanofibers as a promising sensing material for SF_6 decomposition component H_2S were proposed and prepared. The crystal structure and morphology of the electrospun ZnO-SnO_2 samples were investigated by X-ray diffraction (XRD), scanning electron microscopy (SEM) and transmission electron microscopy (TEM), respectively. The composition of the sensitive materials was analyzed by energy dispersive X-ray spectrometers (EDS) and X-ray photoelectron spectroscopy (XPS). Side heated sensors were fabricated with the electrospun ZnO-SnO_2 nanofibers and the gas sensing behaviors to H_2S gas were systematically investigated. The proposed ZnO–SnO_2 composite nanofibers sensor showed lower optimal operating temperature, enhanced sensing response, quick response/recovery time and good long-term stability against H_2S. The measured optimal operating temperature of the ZnO–SnO_2 nanofibers sensor to 50 ppm H_2S gas was about 250°C with a response of 66.23, which was 6 times larger than pure SnO_2 nanofibers sensor. The detection limit of the fabricated ZnO–SnO_2 nanofibers sensor toward H_2S gas can be as low as 0.5 ppm. Finally, a plausible sensing mechanism for the proposed ZnO–SnO_2 composite nanofibers sensor to H_2S was also discussed.

Keywords: ZnO-SnO_2 nanofibers, electrospinning, H_2S, sensing properties, SF_6 decomposition components

OPEN ACCESS

Edited by:
Zhongchang Wang,
Laboratório Ibérico Internacional de Nanotecnologia (INL), Portugal

Reviewed by:
Yong Zhang,
Xiangtan University, China
Qi Qi,
Jilin University, China

****Correspondence:***
Qu Zhou
zhouqu@swu.edu.cn
Caisheng Wang
cwang@wayne.edu

Specialty section:
This article was submitted to Nanoscience, a section of the journal Frontiers in Chemistry

Received: *27 August 2018*
Accepted: *18 October 2018*
Published: *06 November 2018*

Citation:
Lu Z, Zhou Q, Wang C, Wei Z, Xu L and Gui Y (2018) Electrospun ZnO–SnO_2 Composite Nanofibers and Enhanced Sensing Properties to SF_6 Decomposition Byproduct H_2S. Front. Chem. 6:540. doi: 10.3389/fchem.2018.00540

INTRODUCTION

Sulfur hexafluoride (SF_6) insulating gas has excellent insulation performance and arc quenching. It is widely applied in gas-insulated switchgear (GIS) of power system as electrical insulator as well as arc-quenching medium (Beroual and Haddad, 2017; Zhang X. et al., 2017). However, partial discharge and disruptive discharge might occur in GIS equipment during the long run, accounting for the SF_6 gas decomposing to various decomposition components, such as H_2S, SO_2, SOF_2, SO_2F_2 (Tsai, 2007; Liu et al., 2017). Previous researches have reported that these typical decomposition components are able to accelerate the corrosion rate of the GIS equipment and increase the paralysis possibility of the power system (Zhang X. et al., 2016; Li et al., 2017). Therefore, accurate and effective detection of SF_6 gas decomposition components is significant to estimate and optimize the operation state of GIS power equipment.

Semiconductor metal oxides such as SnO_2 (Qi et al., 2014; Li et al., 2016; Shahabuddin et al., 2017; Zhou et al., 2018a), ZnO (Zhou et al., 2013; Zuo et al., 2013; Zhu et al., 2018), TiO_2 (Zeng et al., 2012; Park et al., 2017; Zhang Y. X. et al., 2018), NiO (Zhang Y. et al., 2016; Zhou et al., 2018b,c) are the most investigated group for gas sensors owing to their outstanding gas response and selectivity. Sensing nanostructure with high surface area and full electron depletion is advantageous to enhance the sensing performances (Hao et al., 2012; Miller et al., 2014). In particular, the 1D nanostructures such as nanofibers (Jiang et al., 2016), nanorods (Zhang et al., 2014; Zou et al., 2016), and nanotubes (Kong et al., 2015) have been extensively applied to improve gas sensing properties (Li T. M. et al., 2015; Long et al., 2018). Besides, many studies indicated that the selectivity and other important sensing parameters of semiconductor metal oxide nanomaterials can be enhanced by compositing semiconductor metal oxides (Zhou et al., 2015; Tomer and Duhan, 2016; Wang et al., 2017). Jae-Hun Kim et al. systematically investigated the sensing applications of $xSnO_2$-$(1-x)Co_3O_4$ composite nanofibers and reported that the $0.5SnO_2$-$0.5Co_3O_4$ sensor exhibited the most outstanding sensing characteristics (Kim et al., 2017). As one of the most important decomposition components of SF_6, H_2S has been widely studied in the past few years. A variety of composite metal oxides like Cu_2O-SnO_2 (Cui et al., 2013), CeO-SnO_2 (Fang et al., 2000), NiO-ZnO (Qu et al., 2016), and PdO-NiO (Balamurugan et al., 2017) have been reported as promising materials for H_2S gas sensing applications. However, the report of ZnO-SnO_2 composite nanofibers for H_2S gas sensing has been only investigated in a limited number of reports.

In this present work, we have successfully synthesized ZnO-SnO_2 nanofibers by electrospinning method and systematically investigated their sensing performances to H_2S gas. The prepared ZnO-SnO_2 nanofibers exhibited significantly improved sensing properties containing high response, low detection limit, low operating temperature and fast response/recovery times to H_2S gas detection, which can be ascribed to the large surface area of nanofiber structure and the formation of n-n heterojunctions at interface between ZnO and SnO_2. Finally, a plausible sensing mechanism for the proposed ZnO–SnO_2 composite nanofibers sensor to H_2S was also discussed.

EXPERIMENTAL

Materials Synthesis

Zinc nitrate hexahydrate ($Zn(NO_3)_2{\cdot}6H_2O$), stannic chloride pentahydrate ($SnCl_4{\cdot}5H_2O$), N,N-dimethylformamide (DMF), polyvinylpyrrolidone (PVP, Mw = 1,300,000) and ethanol were of analytical graded and used directly without further purification. All chemicals were purchased from Chongqing Chuandong Chemical Reagent Co., Ltd (Lu et al., 2018).

In the typical synthesis of ZnO-SnO_2 composite nanofibers, 0.7 g of $SnCl_4{\cdot}5H_2O$ and 0.6 g $Zn(NO_3)_2{\cdot}6H_2O$ (the molar ratio was 1:1) were dissolved in 5 ml of mixed solvents of ethanol and DMF (The volume ratio was 1:1) and stirred for 2 h. Then 2 g of PVP was added to the mixture and stirred for 24 h to form a viscous and homogeneous solution at room temperature. During electrospinning, the obtained mixture was delivered to a glass syringe. A voltage of 25 kV was applied between the flat aluminum foil and syringe at an electrode distance of 15 cm as shown in **Figure 1** and the flow rate is 0.7 ml/h. Finally, the electrospun nanofibers were transferred to a tube furnace and the specimens were annealed at 600°C for 3 h in air for the removal of PVP. For comparison, the pure SnO_2 nanofibers were also synthesized without adding $Zn(NO_3)_2{\cdot}6H_2O$. The schematic illustration of producing electrospun ZnO-SnO_2 composite nanofibers was shown in **Figure 1** (Bai et al., 2018).

Materials Characterization

To investigate the structures of electrospun ZnO-SnO_2 nanofibers, X-ray diffraction (XRD, D/Max-1200X, Rigaku, Japan) analysis was carried out at room temperature using a Rigaku D/Max-1200X diffractometry with Cu-Kα radiation (λ = 1.542 Å) over Bragg angles from 20° to 75° and the scanning speed of 2 deg/min. The morphologies of the electrospun nanofibers were investigated with a field emission scanning electronic microscopy (FESEM, JSM-6700F, JEOL, Japan) and transmission electron microscopy (TEM, JEM-2100, JEOL, Japan) operated at 120 kV. The energy dispersive X-ray spectrum analysis (EDS, Oxford INCA 250, JEOL, Japan) and X-ray photoelectron spectroscopy analysis (XPS, KRATOS X SAM800, Kratos, Kingdom) were tested to analyze the elemental compositions of the sample (Lu et al., 2018).

Gas Sensor Measurements

Gas sensors were fabricated with a side heated structure as shown in **Figure 2A** and a theoretic diagram of the test circuit was showed in **Figure 2B**. As shown in **Figure 2A**, there are two gold electrodes connected with platinum wire at both ends of the ceramic tube. Firstly, the as-prepared powder was mixed with appropriate amount of anhydrous ethanol and deionized water to form a homogeneous paste (Xu et al., 2015). Then the obtained paste was coated onto a prefabricated ceramic tube to form the sensing film and dried at room temperature for 2 h. Next a Ni–Cr heating wire was inserted into the ceramic tube to finish the side heated H_2S gas sensor. Finally, the stability of the sensing materials was improved by putting the sensor on the aging instrument of the side heated sensor at 120°C for 10 days. The sensor response was defined as $S = R_a/R_g$ (Zhang Q. Y. et al., 2017), where R_a and R_g were the resistances of the sensing material measured in air and in atmosphere containing target test gas H_2S, respectively (Zhu et al., 2017). Gas sensing properties of the obtained sensors were performed with the CGS-8 TP intelligent gas sensing analysis system (Chemical gas sensor-8, Beijing Elite Tech Co., Ltd., China). The response time was defined as the time required by the sensor to reach 90% of the final stable resistance when target gas in. The recovery time is the time required to return to 90% of its original baseline resistance when the sensor was exposed in air again (Nan et al., 2017). The sensing measurement were tested under laboratory condition with room temperature 25°C and constant humidity (50% relative humidity).

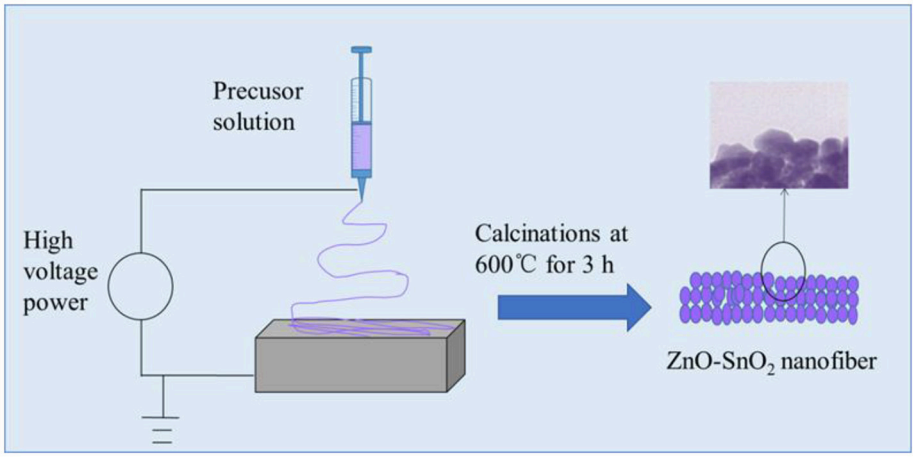

FIGURE 1 | Schematic illustration of producing electrospun ZnO-SnO_2 nanofibers.

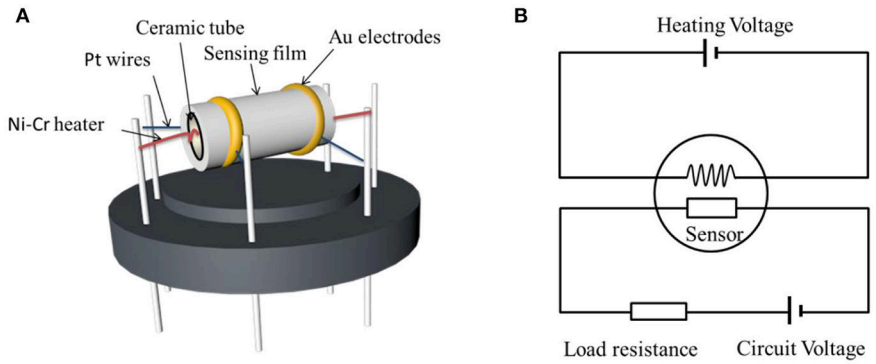

FIGURE 2 | (A) Schematic structure of the ZnO-SnO_2 nanofibers gas sensor and **(B)** theoretic diagram of the test circuit.

RESULTS AND DISCUSSION

Morphology and Structure

Figure 3 shows the XRD pattern of the electrospun ZnO-SnO_2 composite nanofibers. It can be seen from **Figure 3** that the XRD peaks are in accordance with the hexagonal wurtzite ZnO and tetragonal rutile SnO_2, compared with the standard pattern of JCPDS card No. 36-1451 and No. 41-1445, respectively. There is neither apparent peak shift nor any other phase corresponding SnO, $ZnSnO_3$ and Zn_2SnO_4, confirming that there are only SnO_2 and ZnO co-exist in the prepared material. The result shows a possibility of developing n–n heterojunction at the interface between ZnO and SnO_2 nanomaterial (Bai et al., 2018). The crystallite sizes of nanoparticels were calculated using Scherrer's equation ($D = k\lambda/\beta\cos\theta$) (Lu et al., 2018), and the average crystallite sizes of nanofibers were calculated by diffraction peaks (100), (101) for ZnO, and (110), (101), (221) for SnO_2. After calculation, the average crystallite size of ZnO is 20.1 nm, while it is 19.8 nm of SnO_2.

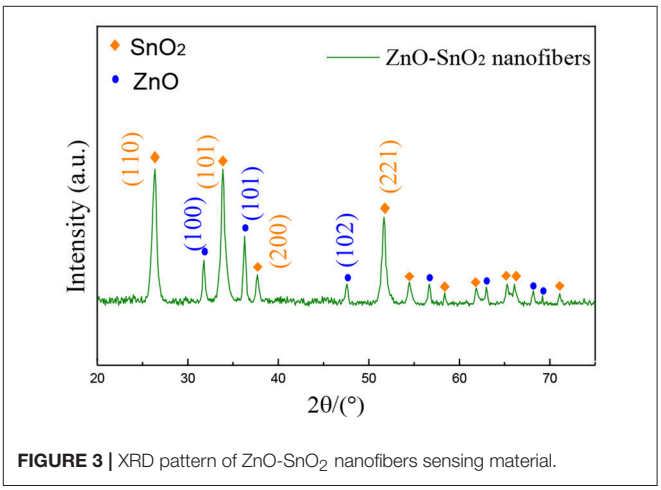

FIGURE 3 | XRD pattern of ZnO-SnO_2 nanofibers sensing material.

Figure 4 presents the FESEM and TEM images of the as-prepared ZnO-SnO_2 nanofibers after annealing. **Figure 4a** consists of randomly oriented nanofibers with diameters of 80–150 nm and lengths of 0.5–2 μm. Besides, the ZnO-SnO_2 nanofibers consist of nanoparticles and surface of nanofibers

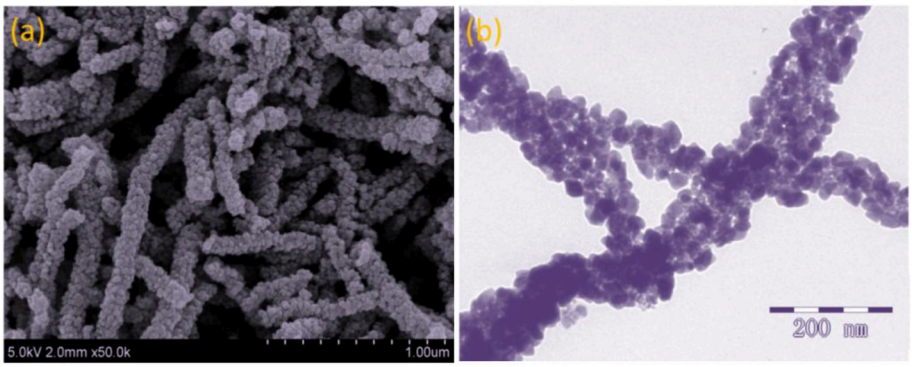

FIGURE 4 | (a) FESEM image and **(b)** TEM image of electrospun ZnO-SnO_2 nanofibers.

is rough, which can be attributed to thermal decomposition of PVP caused by annealing. More structural information of the ZnO-SnO_2 nanofibers is researched by TEM characterization as shown in **Figure 4b**, the single fiber is composed of grain-like nanoparticles with around 20 nm in size.

Figure 5 demonstrates the EDS spectrum of the electrospun ZnO-SnO_2 nanofibers. It can be seen that the ZnO–SnO_2 composite nanofibers are composed of Zn, Sn, and O elements and the atomic ratio of Zn and Sn is about 19.63:20.76.

To further analyze the compositions and element valences of the ZnO-SnO_2 nanofibers, XPS tests were investigated. **Figure 6A** shows the full range XPS survey spectra of the sample. It confirms the presence of Zn, O, Sn from prepared nanomaterial and C element which is due to the carbon contamination. The binding energies were calibrated using C 1 s hydrocarbon peak at 284.54 eV. **Figures 6B**,**C** demonstrate the high resolution spectra of the Zn 2p and Sn 3d energy state, respectively. The Zn 2p XPS spectrum (**Figure 6B**) presents the doublet peaks located at binding energies of 1045.6 eV and 1022.6eV, which corresponds to Zn $2p_{1/2}$ and Zn $2p_{3/2}$, respectively (Li W. Q. et al., 2015). The result indicates that the Zn^{2+} is the dominant species in the prepared material and in good agreement with the reported data for ZnO (Zhao et al., 2015). **Figure 6C** shows the binding energy of Sn $3d_{5/2}$, Sn $3d_{3/2}$ are 487.6eV and 496.1eV respectively, which are assigned to the highest oxidation state of Sn^{4+} for SnO_2 (Hamrouni et al., 2014; Chen et al., 2018). It further confirmed that ZnO and SnO_2 coexist in the samples.

Gas-Sensing Properties

The gas sensor responses of pure SnO_2 and ZnO-SnO_2 nanofibers sensors as a function of temperatures in the range of 100–375°C toward 50 ppm of H_2S gas were tested and shown in **Figure 7**. The sensing responses of all the prepared sensors increase with increasing temperature and attain a maximum value at 300 and 250°C for pure SnO_2 and ZnO-SnO_2 nanofibers sensor, respectively. With further increase in temperature, the sensing responses begin to decrease because desorption of H_2S is dominated and the amount of the adsorbed gas onto the surface decreases (Zhang et al., 2018). The response of gas sensor based on ZnO-SnO_2 nanofibers for 50 ppm H_2S gas at operating

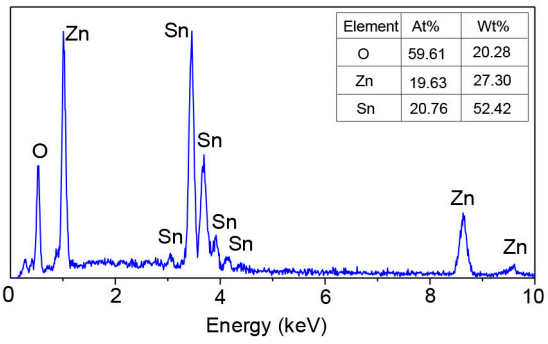

FIGURE 5 | EDS pattern of electrospun ZnO-SnO_2 nanofibers sample.

temperature of 250°C is 66.23, while it is 10.49 and 300°C for the pure SnO_2 nanofibers based sensor. The results indicate that ZnO-SnO_2 composite nanofibers can obviously improve the response to H_2S at different working temperatures and reduce the optimal operating temperature.

Figure 8 shows the H_2S gas responses of pure SnO_2 and ZnO-SnO_2 nanofibers based sensors to different concentration of H_2S in the range of 0.5–100 ppm at their optimal operating temperatures measured above. The measured results show that gas responses of the as-prepared gas sensors increase in a good linear relationship from 0.5 to 100 ppm. The linear relationship of the response and gas concentration satisfies linear equation $y = 1.1003x+6.90664$ for electrospun ZnO-SnO_2 nanofibers gas sensor. The higher response of ZnO-SnO_2 nanofibers can be explained by the formation of n-n heterojunctions at the interface between ZnO and SnO_2. Moreover, the sensor detection limit was defined as the target gas concentration value at which the response is above 3. The response of the ZnO-SnO_2 nanofibers sensor to 0.5 ppm H_2S gas can reach up to 3.45, indicating that the detection limit of the sensor for detecting H_2S gas is as low as sub-ppm level.

The dynamic response and recovery curve of the ZnO-SnO_2 nanofibers sensor for 1, 5, 30, and 50 ppm H_2S gas was performed and shown in **Figure 9**. The obtained sensing response values

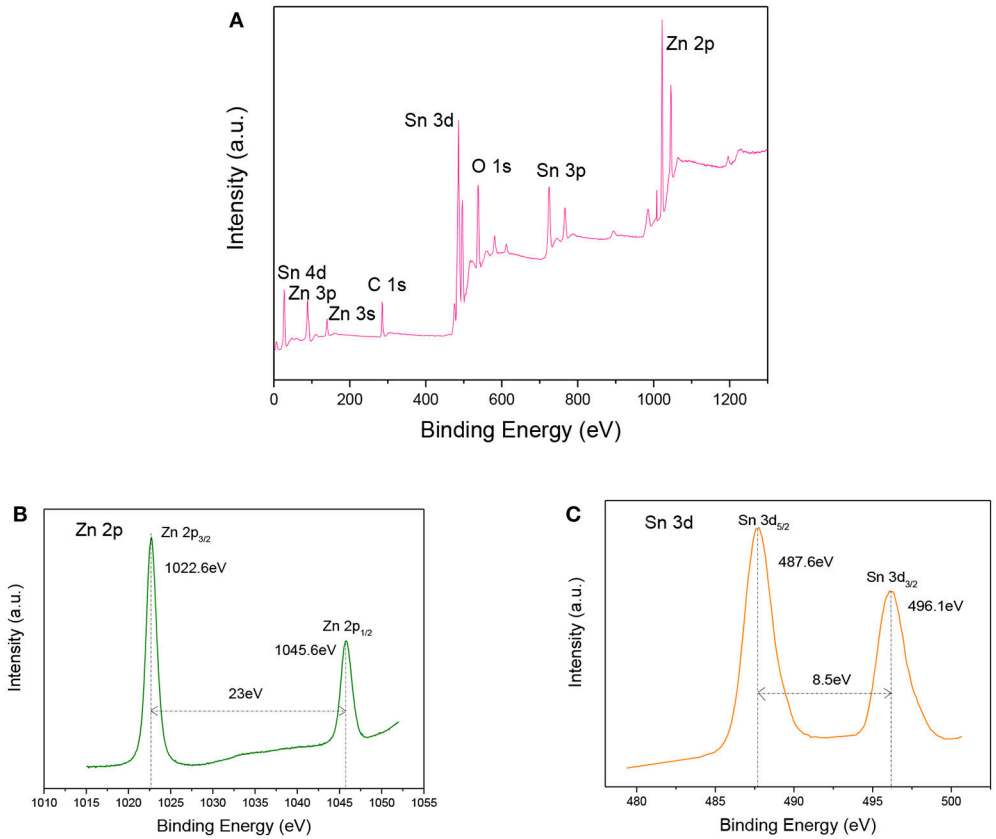

FIGURE 6 | (A) Survey, **(B)** Zn 2p, **(C)** Sn 3d XPS spectra of electrospun ZnO–SnO_2 nanofibers.

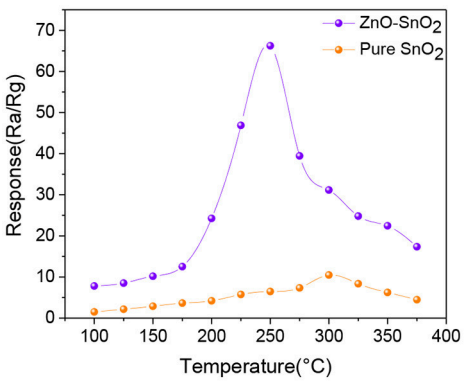

FIGURE 7 | Response to 50 ppm H_2S at different operating temperature of SnO_2 and ZnO-SnO_2 nanofibers sensors.

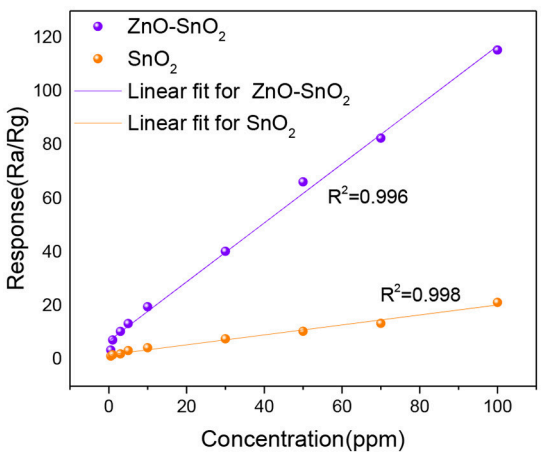

FIGURE 8 | Gas responses for H_2S gas (0.5–100 ppm) using pure SnO_2 and ZnO-SnO_2 nanofibers sensors at their optimal working temperature.

are about 7.25, 13.37, 40.31, and 66.23, respectively. The ZnO-SnO_2 nanofibers sensor responds rapidly and could recover to its initial value when it was exposed to air again, implying a satisfying stability and reproducibility of the proposed H_2S gas sensor.

Figures 10A,**B** illustrate the response-recovery curve of electrospun ZnO-SnO_2 nanofibers sensor and pure SnO_2 nanofibers sensor to 50 ppm of H_2S gas at their optimal operating temperature mentioned above. From the curves, it is observed that the response and recovery time of the ZnO-SnO_2 nanofibers sensor is about 18 and 32 s, respectively, whereas for pure

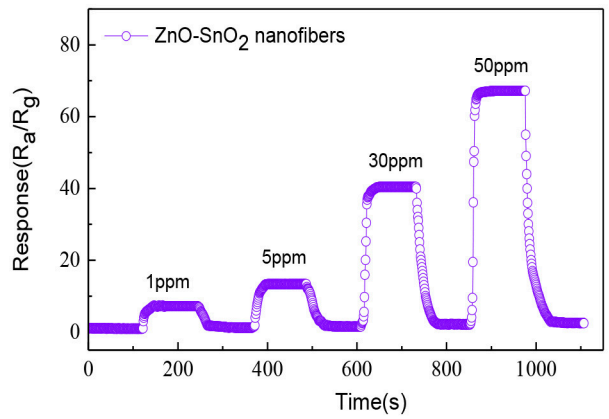

FIGURE 9 | Dynamic response-recovery curve of the sensor based upon ZnO-SnO_2 nanofibers at 250°C.

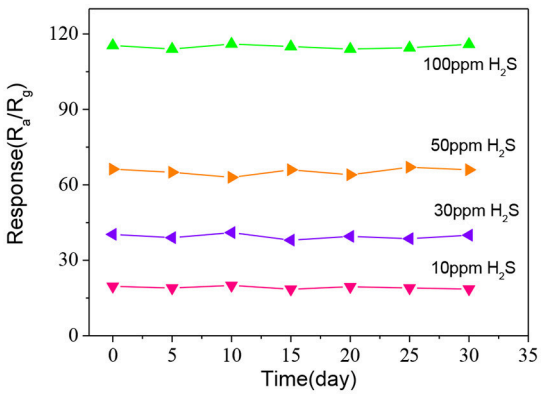

FIGURE 11 | Long term stability property of ZnO-SnO_2 nanofibers sensor.

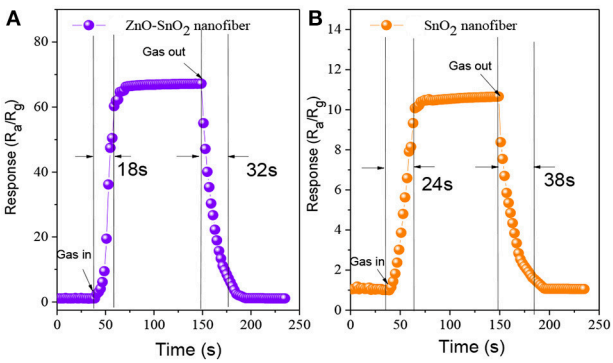

FIGURE 10 | Response-recovery curve of the sensor bases on **(A)** ZnO-SnO_2 nanofibers **(B)** pure SnO_2 nanofibers.

SnO_2 nanofibers sensor the corresponding values is 24 and 38 s, respectively.

Finally, the long-term stability of the fabricated ZnO-SnO_2 nanofibers sensor was measured to 10, 30, 50, and 100 ppm H_2S gas at 250°C for 30 days as shown in **Figure 11**. The measured results show that the response has little change for 30 days and confirm a good stability of the fabricated electrospun ZnO-SnO_2 nanofibers sensor.

Experimental results of ZnO-SnO_2 nanofibers sensor have been compared with the results reported by the other workers on H_2S sensors and presented in **Table 1**. It can be seen that electrospun ZnO-SnO_2 nanofibers sensor toward H_2S can reach a relatively higher response at lower temperature and the response time is relatively shorter than other sensors reported previously. The obtained results indicate that the electrospun ZnO-SnO_2 nanofibers sensor is promising for H_2S gas sensing.

Sensing Mechanism

ZnO and SnO_2 belong to typical n-type semiconductors, characterized by their high free carrier concentration (Hong et al., 2017; Zhou et al., 2018d). The gas sensing mechanism of ZnO-SnO_2 nanofibers is shown in **Figure 12**. Due to the sensing mechanism of ZnO-SnO_2 sensor follows the surface controlled type, the gas sensing properties are ascribed to the change of the surface resistance, which controlled by the adsorption and desorption of oxygen on the surface of sensing materials (Wei et al., 2014). When ZnO-SnO_2 nanofibers sensor is exposed to air (**Figure 12A**), the resistance of gas sensor depends on the amount of chemisorbed oxygen species (O^-, O_2^-, and O^{2-}). The free oxygen molecules are absorbed on the surface and capture electrons from the conduction band of the ZnO-SnO_2 nanofibers, which causes a depletion layer around the surface and the increasing the resistance (Cheng et al., 2014). When ZnO-SnO_2 nanofibers sensing materials are exposed to H_2S (**Figure 12B**), the target gas reacts with the adsorbed oxygen and then releases the captured electrons into the conduction band of ZnO-SnO_2 nanifibers to reduce the depletion layer and decrease the resistance.

It is well-known that the chemisorbed oxygen depends on the specific surface area of sensing materials and the operating temperature. ZnO-SnO_2 nanofibers show a big surface area as shown in **Figure 4**. It means that adsorption capability of ZnO-SnO_2 nanofibers was greatly enhanced (Zhang W. et al., 2017). Moreover, O^{2-} and O^- species are regarded as the most oxygen adsorption species at 250°C, and the following H_2S sensing reaction can be considered (Kolhe et al., 2017).

$$H_2S + 3O^- \rightarrow SO_2 + H_2O + 3e^- \quad (1)$$

$$H_2S + 3O^{2-} \rightarrow SO_2 + H_2O + 6e^- \quad (2)$$

In accordance with the definition about gas response ($S = R_a/R_g$), the increasing of R_a and decreasing of R_g cause that the response of ZnO-SnO_2 nanofibers is significantly enhanced. Additional electron consumption will occur at the boundaries of ZnO and SnO_2, which further enhances the gas response. The contact of ZnO and SnO_2 provides condition for electrons transfer from SnO_2 to ZnO, which has a higher work function of 5.2 eV compared to SnO_2 (4.9 eV). It results in the formation

TABLE 1 | Summary of the H_2S gas sensing performances of different gas sensor materials.

Sensor	H_2S (ppm)	Temp. (°C)	Response (R_a/R_g)	τ_{res} and τ_{rec}	References
Zn_2SnO_4 hollow octahedra	50	260	46	10 and 25 s	Ma et al., 2012
V doped In_2O_3	50	90	14	15 and 18 s	Liu et al., 2014
Co_3O_4-SWCNT composites	100	250	51	>100 s	Moon et al., 2016
Al-ZnO thin film	600	200	30	90 and 209 s	Kolhe et al., 2018
CuO-functionalized WO_3 nanowires	100	300	79.8	~30 and 20 s	Park et al., 2014
Fe_2O_3 -NiO nanoplate	200	200	26	11 and 18 s	Sun et al., 2016
TiO_2/SiO_2 composite aerogel film	50	250	13.5	21 and 600 s	Yang et al., 2018
micro/nanostructured In_2O_3 porous thin	50	300	30	16 and 30 s	Wang et al., 2016
Gold functionalized MoO_3 nano flake	15	400	260	60 and 480 s	Munasinghe Arachchige et al., 2018
ZnO-SnO_2 nanofibers	50	250	66.23	18 and 32 s	This work

Temp., the optimal working temperature. τ_{res} and τ_{rec} - response time and recovery time.

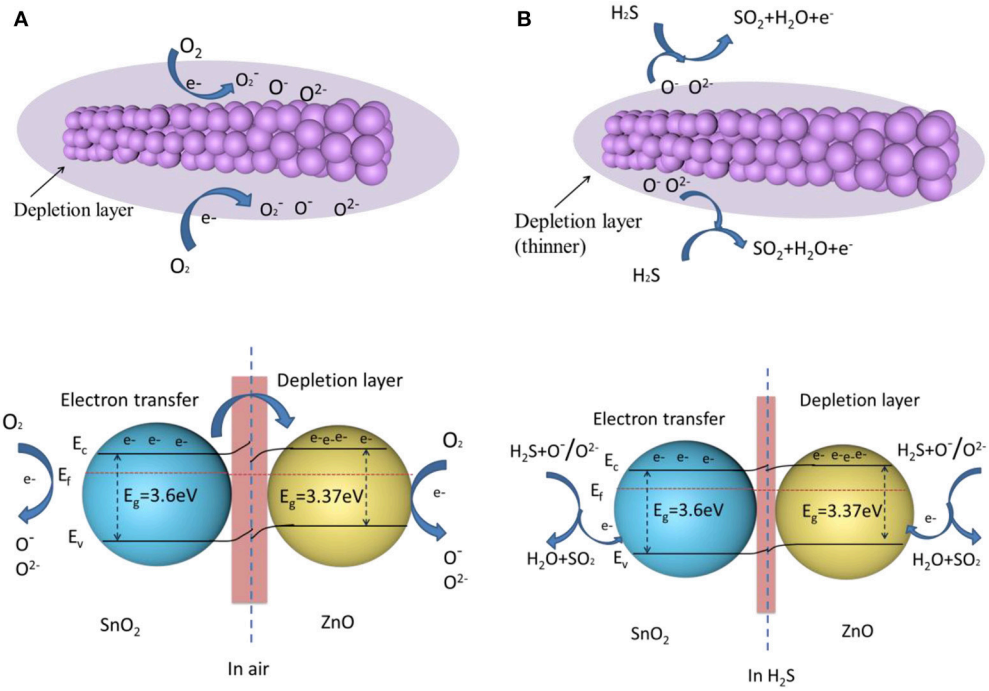

FIGURE 12 | A schematic of the H_2S sensing mechanism of the ZnO-SnO_2 nanofibers **(A)** when the gas sensor is exposed in air **(B)** when the gas sensor is exposed in H_2S (E_f is Fermi level; E_c is conduction band; E_v is valence band; E_g is band gaps).

of an additional depletion layer in the vicinity region between the ZnO and SnO_2, eventually generating a potential barrier for electron flow (Choi et al., 2013). The boundary barrier may decrease when the gas sensor is exposed in H_2S. More electrons of oxygen species transfer to the sensing material by reaction of H_2S with oxygen species, which results the resistance of the sensing material decreases and the response of the sensor increases. However, pure SnO_2 does not provide reaction interface, leading to lower gas response. So the ZnO–SnO_2 composite nanofibers exhibit better sensing properties than the SnO_2 nanofibers.

CONCLUSIONS

In summary, ZnO-SnO_2 composite nanofibers were successfully synthesized by electrospinning method and characterized by various techniques. H_2S sensing properties of the electrospun nanofibers sensor were also investigated. Compared to the pure SnO_2 nanofiber sensor, the ZnO-SnO_2 composite nanofibers sensor shows excellent gas sensing response for H_2S gas, which is attributed to the large specific surface and the heterojunctions between SnO_2 and ZnO. The proposed ZnO-SnO_2 composite

nanofibers sensor exhibits good linear relationship between sensing response and gas concentration in the range of 0.5∼100 ppm and its detection limit is as low as sub-ppm level. Moreover, the proposed sensor achieves good repeatability and long-term stability, making it a promising candidate for detecting H_2S gas.

AUTHOR CONTRIBUTIONS

ZL and ZW performed the experiments and analyzed the data with the help from LX and YG. ZL, QZ, and CW wrote and revised the manuscript with input from all authors. All authors read and approved the manuscript.

ACKNOWLEDGMENTS

This work has been supported in part by the National Natural Science Foundation of China (No. 51507144), the China Postdoctoral Science Foundation Project (Nos. 2015M580771, 2016T90832), the Chongqing Science and Technology Commission (CSTC) (No. cstc2016jcyjA0400) and the project of China Scholarship Council (CSC).

REFERENCES

Bai, S. L., Fu, H., Zhao, Y. Y., Tian, K., Luo, R. X., Li, D. Q., et al. (2018). On the construction of hollow nanofibers of ZnO-SnO_2 heterojunctions to enhance the NO_2 sensing properties. *Sensor. Actuat. B Chem.* 266, 692–702. doi: 10.1016/j.snb.2018.03.055

Balamurugan, C., Jeong, Y. J., and Lee, D. W. (2017). Enhanced H_2S sensing performance of a p-type semiconducting PdO-NiO nanoscale heteromixture. *Appl. Surf. Sci.* 420, 638–650. doi: 10.1016/j.apsusc.2017.05.166

Beroual, A., and Haddad, A. (2017). Recent advances in the quest for a new insulation gas with a low impact on the environment to replace sulfur hexafluoride (SF_6) gas in high-voltage power network applications. *Energies* 10:1216. doi: 10.3390/en10081216

Chen, Y., Qin, H., and Hu, J. (2018). CO sensing properties and mechanism of Pd doped SnO_2 thick-films. *Appl. Surf. Sci.* 428, 207–217. doi: 10.1016/j.apsusc.2017.08.205

Cheng, L., Ma, S. Y., Li, X. B., Luo, J., Li, W. Q., Li, F. M., et al. (2014). Highly sensitive acetone sensors based on Y-doped SnO_2 prismatic hollow nanofibers synthesized by electrospinning. *Sensor. Actuat. B-Chem.* 200, 181–190. doi: 10.1016/j.snb.2014.04.063

Choi, S.-W., Katoch, A., Sun, G.-J., and Kim, S. S. (2013). Synthesis and gas sensing performance of ZnO–SnO_2 nanofiber–nanowire stem-branch heterostructure. *Sensor. Actuat. B Chem.* 181, 787–794. doi: 10.1016/j.snb.2013.02.010

Cui, G., Zhang, M., and Zou, G. (2013). Resonant tunneling modulation in quasi-2D Cu_2O/SnO_2 p-n horizontal-multi-layer heterostructure for room temperature H_2S sensor application. *Sci. Rep.* 3:1250. doi: 10.1038/srep01250

Fang, G. J., Liu, Z. L., Liu, C. Q., and Yao, K. L. (2000). Room temperature H_2S sensing properties and mechanism of CeO_2-SnO_2 sol-gel thin films. *Sensor. Actuat. B-Chem.* 66, 46–48. doi: 10.1016/S0925-4005(99)00467-0

Hamrouni, A., Moussa, N., Parrino, F., Di Paola, A., Houas, A., and Palmisano, L. (2014). Sol–gel synthesis and photocatalytic activity of ZnO–SnO_2 nanocomposites. *J. Mol. Catal. A Chem.* 390, 133–141. doi: 10.1016/j.molcata.2014.03.018

Hao, D., Zhu, J. H., Jiang, J., Ding, R. M., Feng, Y. M., Wei, G. M., et al. (2012). Preparation and gas-sensing property of ultra-fine NiO/SnO2 nano-particles. *RSC Adv.* 2:10324–10329. doi: 10.1039/C2RA21121A

Hong, C., Zhou, Q., Lu, Z., Umar, A., Kumar, R., Wei, Z., et al. (2017). Ag-doped ZnO nanoellipsoids based highly sensitive gas sensor. *Mater. Exp.* 7, 380–388. doi: 10.1166/mex.2017.1388

Jiang, Z., Zhao, R., Sun, B., Nie, G., Ji, H., Lei, J., et al. (2016). Highly sensitive acetone sensor based on Eu-doped SnO_2 electrospun nanofibers. *Ceram. Int.* 42, 15881–15888. doi: 10.1016/j.ceramint.2016.07.060

Kim, J.-H., Lee, J.-H., Mirzaei, A., Kim, H. W., and Kim, S. S. (2017). Optimization and gas sensing mechanism of n-SnO_2-p-Co_3O_4 composite nanofibers. *Sensor. Actuat. B-Chem.* 248, 500–511. doi: 10.1016/j.snb.2017.04.029

Kolhe, P. S., Koinkar, P. M., Maiti, N., and Sonawane, K. M. (2017). Synthesis of Ag doped SnO_2 thin films for the evaluation of H_2S gas sensing properties. *Phys. B Condensed Matter.* 524, 90–96. doi: 10.1016/j.physb.2017.07.056

Kolhe, P. S., Shinde, A. B., Kulkarni, S. G., Maiti, N., Koinkar, P. M., and Sonawane, K. M. (2018). Gas sensing performance of Al doped ZnO thin film for H_2S detection. *J. Alloy. Compd.* 748, 6–11. doi: 10.1016/j.jallcom.2018.03.123

Kong, J., Rui, Z., Ji, H., and Tong, Y. (2015). Facile synthesis of ZnO/SnO_2 hetero nanotubes with enhanced electrocatalytic property. *Catal. Today* 258, 75–82. doi: 10.1016/j.cattod.2015.04.011

Li, L., Fan, X. P., Zhou, Y. Y., Tang, N., Zou, Z. L., Liu, M. Z., et al. (2017). Research on technology of online gas chromatograph for SF_6 decomposition products. *IOP Conf. Ser. Mater. Sci. Eng.* 274, 012–038. doi: 10.1088/1757-899X/274/1/012038

Li, T., Zeng, W., Long, H., and Wang, Z. (2016). Nanosheet-assembled hierarchical SnO_2 nanostructures for efficient gas-sensing applications. *Sensor. Actuat. B-Chem.* 231, 120–128. doi: 10.1016/j.snb.2016.03.003

Li, T. M., Zeng, W., and Wang, Z. C. (2015). Quasi-one-dimensional metal-oxide-based heterostructural gas-sensing materials: a review. *Sensor. Actuat. B-Chem.* 221, 1570–1585. doi: 10.1016/j.snb.2015.08.003

Li, W. Q., Ma, S. Y., Li, Y. F., Yang, G. J., Mao, Y. Z., Luo, J., et al. (2015). Enhanced ethanol sensing performance of hollow ZnO–SnO2 core–shell nanofibers. *Sensor. Actuat. B Chem.* 221, 392–402. doi: 10.1016/j.snb.2015.01.090

Liu, H. C., Zhou, Q., Zhang, Q. Y., Hong, C. X., Xu, L. N., Jin, L. F., et al. (2017). Synthesis, characterization and enhanced sensing properties of a NiO/ZnO p-n junctions sensor for the SF_6 decomposition byproducts SO_2, SO_2F_2, and SOF_2. *Sensors* 17:913. doi: 10.3390/s17040913

Liu, J., Guo, W., Qu, F., Feng, C., Li, C., Zhu, L., et al. (2014). V-doped In_2O_3 nanofibers for H_2S detection at low temperature. *Ceram. Int.* 40, 6685–6689. doi: 10.1016/j.ceramint.2013.11.129

Long, H. W., Zeng, W., Wang, H., Qian, M. M., Liang, Y. H., and Wang, Z. C. (2018). Self-Assembled biomolecular 1D nanostructures for aqueous sodium-ion battery. *Adv. Sci.* 5:1700634. doi: 10.1002/advs.201700634

Lu, Z., Zhou, Q., Xu, L., Gui, Y., Zhao, Z., Tang, C., et al. (2018). Synthesis and characterization of highly sensitive hydrogen (H2) sensing device based on Ag doped SnO2 nanospheres. *Materials* 11:E492. doi: 10.3390/ma11040492

Ma, G., Zou, R., Jiang, L., Zhang, Z., Xue, Y., Yu, L., et al. (2012). Phase-controlled synthesis and gas-sensing properties of zinc stannate ($ZnSnO_3$ and Zn_2SnO_4) faceted solid and hollow microcrystals. *CrystEngComm* 14, 2172–2179. doi: 10.1039/c2ce06272k

Miller, D. R., Akbar, S. A., and Morris, P. A. (2014). Nanoscale metal oxide-based heterojunctions for gas sensing: a review. *Sensor. Actuat. B Chem.* 204, 250–272. doi: 10.1016/j.snb.2014.07.074

Moon, S., Vuong, N. M., Lee, D., Kim, D., Lee, H., Kim, D., et al. (2016). Co_3O_4-SWCNT composites for H_2S gas sensor application. *Sensor. Actuat. B Chem.* 222, 166–172. doi: 10.1016/j.snb.2015.08.072

Munasinghe Arachchige, H. M. M., Zappa, D., Poli, N., Gunawardhana, N., and Comini, E. (2018). Gold functionalized MoO_3 nanoflakes for gas sensing applications. *Sensor. Actuat. B Chem.* 269, 331–339. doi: 10.1016/j.snb.2018.04.124

Nan, C., Li, Y. X., Deng, D. Y., Xu, L.,Xing, X. X., Xiao, X. C., et al. (2017). Acetone sensing performances based on nanoporous TiO_2 synthesized by a facile hydrothermal method. *Sensor. Actuat. B Chem.* 238, 491–500. doi: 10.1016/j.snb.2016.07.094

Park, J. Y., Kim, H. H., Rana, D., Jamwal, D., and Katoch, A. (2017). Surface-area-controlled synthesis of porous TiO_2 thin films for gas-sensing applications. *Nanotechnology* 28:095502. doi: 10.1088/1361-6528/aa5836

Park, S., Park, S., Jung, J., Hong, T., Lee, S., Kim, H. W., et al. (2014). H_2S gas sensing properties of CuO-functionalized WO_3 nanowires. *Ceram. Int.* 40, 11051–11056. doi: 10.1016/j.ceramint.2014.03.120

Qi, Q., Wang, P.-P., Zhao, J., Feng, L.-L., Zhou, L.-J., Xuan, R.-F., et al. (2014). SnO_2 nanoparticle-coated In_2O_3 nanofibers with improved NH3 sensing properties. *Sensor. Actuat. B Chem.* 194, 440–446. doi: 10.1016/j.snb.2013.12.115

Qu, Z., Fu, Y., Yu, B., Deng, P., Xing, L., and Xue, X. (2016). High and fast H_2S response of NiO/ZnO nanowire nanogenerator as a self-powered gas sensor. *Sensor. Actuat. B Chem.* 222, 78–86. doi: 10.1016/j.snb.2015.08.058

Shahabuddin, M., Umar, A., Tomar, M., and Gupta, V. (2017). Custom designed metal anchored SnO_2 sensor for H_2 detection. *Int. J. Hydrogen Energ.* 42, 4597–4609. doi: 10.1016/j.ijhydene.2016.12.054

Sun, G.-J., Kheel, H., Lee, J. K., Choi, S., Lee, S., and Lee, C. (2016). H_2S gas sensing properties of Fe_2O_3 nanoparticle-decorated NiO nanoplate sensors. *Surf. Coat. Tech.* 307, 1088–1095. doi: 10.1016/j.surfcoat.2016.06.066

Tomer, V. K., and Duhan, S. (2016). Ordered mesoporous Ag-doped TiO_2/SnO_2 nanocomposite based highly sensitive and selective VOC sensors. *J. Mater. Chem. A* 4, 1033–1043. doi: 10.1039/C5TA08336B

Tsai, W.-T. (2007). The decomposition products of sulfur hexafluoride (SF_6): reviews of environmental and health risk analysis. *J. Fluorine Chem.* 128, 1345–1352. doi: 10.1016/j.jfluchem.2007.06.008

Wang, C., Zeng, W., and Chen, T. (2017). Facile synthesis of thin nanosheet assembled flower-like NiO-ZnO composite and its ethanol-sensing performance. *J. Mater. Sci.* 28, 222–227. doi: 10.1007/s10854-016-5514-1

Wang, Y., Duan, G., Zhu, Y., Zhang, H., Xu, Z., Dai, Z., et al. (2016). Room temperature H_2S gas sensing properties of In_2O_3 micro/nanostructured porous thin film and hydrolyzation-induced enhanced sensing mechanism. *Sensor. Actuat. B Chem.* 228, 74–84. doi: 10.1016/j.snb.2016.01.002

Wei, S. H., Wang, S. M., Zhang, Y., and Zhou, M. H. (2014). Different morphologies of ZnO and their ethanol sensing property. *Sensor. Actuat. B Chem.* 192, 480–487. doi: 10.1016/j.snb.2013.11.034

Xu, L., Chen, N., Han, B. Q., Xiao, X. C., Chen, G., Djerdj, L., et al. (2015). Nanoparticle cluster gas sensor: Pt activated SnO_2 nanoparticles for NH_3 detection with ultrahigh sensitivity. *Nanoscale* 36, 14872–14880. doi: 10.1039/C5NR03585F

Yang, F., Zhu, J., Zou, X., Pang, X., Yang, R., Chen, S., et al. (2018). Three-dimensional TiO_2 /SiO_2 composite aerogel films via atomic layer deposition with enhanced H_2S gas sensing performance. *Ceram. Int.* 44, 1078–1085. doi: 10.1016/j.ceramint.2017.10.052

Zeng, W., Liu, T. M., and Wang, Z. C. (2012). Enhanced gas sensing properties by SnO_2 nanosphere functionalized TiO_2 nanobelts. *J. Mater. Chem.* 22, 3544–3548. doi: 10.1039/c2jm15017d

Zhang, H., Zeng, W., Zhang, Y., Li, Y. Q., Miao, B., Chen, W. G., et al. (2014). Synthesis and gas sensing properties of novel SnO_2 nanorods. *J. Mater. Sci. Mater. El.* 25, 5006–5012. doi: 10.1007/s10854-014-2264-9

Zhang, Q. Y., Zhou, Q., Yin, X. T., Liu, H. C., Xu, L. N., Tan, W. M., et al. (2017). The effect of PMMA pore-forming on hydrogen sensing properties of porous SnO_2 thick film sensor. *Sci. Adv. Mater.* 9, 1350–1355. doi: 10.1166/sam.2017.3111

Zhang, W., Xie, C., Zhang, G., Zhang, J., Zhang, S., and Zeng, D. (2017). Porous $LaFeO_3$/SnO_2 nanocomposite film for CO_2 detection with high sensitivity. *Mater. Chem. Phys.* 186, 228–236. doi: 10.1016/j.matchemphys.2016.10.048

Zhang, X., Cui, H., Gui, Y., and Tang, J. (2017). Mechanism and application of carbon nanotube sensors in SF_6 decomposed production detection: a review. *Nanoscale Res. Lett.* 12:177. doi: 10.1186/s11671-017-1945-8

Zhang, X., Gui, Y., and Dong, X. (2016). Preparation and application of TiO_2 nanotube array gas Sensor for SF_6-insulated equipment detection: a review. *Nanoscale Res. Lett.* 11:302. doi: 10.1186/s11671-016-1516-4

Zhang, Y., Wang, J., Wei, H., Hao, J., Mu, J., Cao, P., et al. (2016). Hydrothermal synthesis of hierarchical mesoporous NiO nanourchins and their supercapacitor application. *Mater. Lett.* 162, 67–70. doi: 10.1016/j.matlet.2015.09.123

Zhang, Y., Zeng, W., and Li, Y. (2018). The hydrothermal synthesis of 3D hierarchical porous MoS_2 microspheres assembled by nanosheets with excellent gas sensing properties. *J. Alloy. Compd.* 749, 355–362. doi: 10.1016/j.jallcom.2018.03.307

Zhang, Y. X., Zeng, W., Ye, H., and Li, Y. Q. (2018). Enhanced carbon monoxide sensing properties of TiO_2 with exposed (001) facet: a combined first-principle and experimental study. *Appl. Surf. Sci.* 442, 507–516. doi: 10.1016/j.apsusc.2018.02.036

Zhao, Y., Li, X., Dong, L., Yan, B., Shan, H., Li, D., et al. (2015). Electrospun SnO_2 –ZnO nanofibers with improved electrochemical performance as anode materials for lithium-ion batteries. *Int. J. Hydrogen Energ.* 40, 14338–14344. doi: 10.1016/j.ijhydene.2015.06.054

Zhou, Q., Chen, W., Xu, L., Kumar, R., Gui, Y., Zhao, Z., et al. (2018a). Highly sensitive carbon monoxide (CO) gas sensors based on Ni and Zn doped SnO_2 nanomaterials. *Ceram. Int.* 44, 4392–4399. doi: 10.1016/j.ceramint.2017.12.038

Zhou, Q., Chen, W., Xu, L., and Peng, S. (2013). Hydrothermal synthesis of various hierarchical ZnO nanostructures and their methane sensing properties. *Sensors* 13, 6171–6182. doi: 10.3390/s130506171

Zhou, Q., Lu, Z., Wei, Z., Xu, L., Gui, Y., and Chen, W. (2018b). Hydrothermal synthesis of hierarchical ultrathin NiO nanoflakes for high-performance CH_4 sensing. *Front. Chem.* 6:194. doi: 10.3389/fchem.2018.00194

Zhou, Q., Tang, C., Zhu, S. P., and Chen, W. G. (2015). NiO doped SnO_2 p-n heterojunction microspheres: preparation, characterisation and CO sensing properties. *Mater. Technol.* 30, 349–355. doi: 10.1179/17535557 15Y.0000000010

Zhou, Q., Umar, A., Sodki, E., Amine, A., Xu, L. N., Gui, Y. G., et al. (2018c). Fabrication and characterization of highly sensitive and selective sensors based on porous NiO nanodisks. *Sensor. Actuat. B. Chem.* 259, 604–615. doi: 10.1016/j.snb.2017.12.050

Zhou, Q., Xu, L., Umar, A., Chen, W., and Kumar, R. (2018d). Pt nanoparticles decorated SnO_2 nanoneedles for efficient CO gas sensing applications. *Sensor. Actuat. B-Chem.* 256, 656–664. doi: 10.1016/j.snb.2017.09.206

Zhu, L., Li, Y. Q., and Zeng, W. (2017). Enhanced ethanol sensing and mechanism of Cr-doped ZnO nanorods: experimental and computational study. *Ceram. Int.* 43, 14873–14879. doi: 10.1016/j.ceramint.2017.08.003

Zhu, L., Zeng, W., Ye, H., and Li, Y. Q. (2018). Volatile organic compound sensing based on coral rock-like ZnO. *Mater. Res. Bull.* 100, 259–264. doi: 10.1016/j.materresbull.2017.12.043

Zou, C. W., Wang, J., and Xie, W. (2016). Synthesis and enhanced NO_2 gas sensing properties of ZnO nanorods/TiO_2 nanoparticles heterojunction composites. *J. Colloid Interf. Sci.* 478, 22–28. doi: 10.1016/j.jcis.2016.05.061

Zuo, Z. J., Wang, L., Liu, Y.-J., and Huang, W. (2013). The effect of CuO–ZnO–Al_2O_3 catalyst structure on the ethanol synthesis from syngas. *Catal. Commun.* 34, 69–72. doi: 10.1016/j.catcom.2013.01.008

Conflict of Interest Statement: The authors declare that the research was conducted in the absence of any commercial or financial relationships that could be construed as a potential conflict of interest.